Sensors and Actuators B 213 (2015) 314–321

Contents lists available at ScienceDirect

Sensors and Actuators B: Chemical

journal homepage: www.elsevier.com/locate/snb

Utilization of both-side metal decoration in close-packed SnO_2 nanodome arrays for ultrasensitive gas sensing

Young-Seok Shim[a,b], Do Hong Kim[b], Hu Young Jeong[c], Yeon Hoo Kim[b], Seung Hoon Nahm[d], Chong-Yun Kang[e,f], Jin-Sang Kim[e], Wooyoung Lee[a,*], Ho Won Jang[b,**]

[a] Department of Materials Science and Engineering, Yonsei University, Seoul 120-749, Republic of Korea
[b] Department of Materials Science and Engineering, Research Institute for Advanced Materials, Seoul National University, Seoul 151-744, Republic of Korea
[c] UCRF, Ulsan National Institute of Science and Technology, Ulsan 689-798, Republic of Korea
[d] Center for Energy Materials Metrology, Korea Research Institute of Standards and Science, Daejeon 305-340, Republic of Korea
[e] Electronic Materials Research Center, Korea Institute of Science and Technology, Seoul 136-791, Republic of Korea
[f] NBIT, KU-KIST Graduate School of Converging Science and Technology, Seoul 136-701, Republic of Korea

ARTICLE INFO

Article history:
Received 3 December 2014
Received in revised form 10 February 2015
Accepted 22 February 2015
Available online 3 March 2015

Keywords:
Nanodome arrays
Metal decoration
Soft-templating
Gas sensor
Ultrasensitive

ABSTRACT

Metal decoration on hollow metal oxide nanostructures is an attractive route to enhance gas sensing properties. Herein, we present a facile method for the utilization of metal decoration on both the inner and outer surfaces of hollow metal oxide nanostructure for the first time. Close-packed SnO_2 nanodome arrays decorated with Au nanoparticles are fabricated by soft-template method and self-agglomeration of an Au film. The position of Au decoration for SnO_2 nanodome arrays is controlled by changing the deposition sequence of Au and SnO_2 films. While inside, outside, and both-side Au-decorated SnO_2 nanodome arrays show much higher responses to various gases than a bare SnO_2 nanodome, it is shown that the response of both-side Au-decorated SnO_2 nanodome arrays to C_2H_5OH at 300 °C is 18 times higher than that of the bare SnO_2 nanodome arrays and the theoretical detection limit is below 1 ppb. These are attributed to the catalytic effect of Au nanoparticles on the modulation of barrier potentials in links between the individual SnO_2 nanodomes. Our results demonstrate that the utilization of both-side metal decoration is an effective strategy for enhancing the gas sensing performance of hollow metal oxide nanostructures.

1. Introduction

Gas sensors are widely used in diverse areas such as automotive, aerospace, domestic, and security industries in order to detect, monitor, and control the harmful, toxic, hazardous, and flammable gases [1–3]. In addition, their applications have been reaching emerging fields such as noninvasive diagnosis of human diseases [4–7]. Recent studies have shown that the various diseases including lung cancer, asthma, diabetes, renal diseases, and halitosis can be diagnosed by detecting gaseous biomarkers such as H_2S, NO_x, and volatile organic compounds from exhaled breath [8–10]. Various gas sensors, including optical sensors, electrochemical sensors, surface acoustic wave sensors, and semiconductor metal oxide sensors have been demonstrated for breath analyser applications [11–13]. Among them, semiconductor gas sensors based on metal oxides are very promising as sensing elements for breath analysers due to their irreplaceable advantages such as cost-effectiveness, simplicity in fabrication, small size, and easy integration with electronic circuits [14,15]. For a semiconductor gas sensor, the gas sensing performance is significantly improved by increasing the surface-to-volume ratio of the sensing film [16]. Accordingly, over the past decade, low dimensional nanomaterials with large specific surface area have been predominantly investigated. Despite the efforts, how to integrate them with low-cost and high-yield mass production process still remains challenging. Also reliable and reproducible gas sensing properties are often hard to be obtained due to nonuniform connections between randomly distributed individual nanomaterials [17,18].

An alternative route to achieve highly sensitive and reliable semiconductor metal oxide gas sensor is the use of soft-templating

* Corresponding author. Tel.: +82 2 2123 2834; fax: +82 2 312 5375.
** Corresponding author. Tel.: +82 880 1720; fax: +82 2 884 1413.
E-mail addresses: wooyouong@yonsei.ac.kr (W. Lee), hwjang@snu.ac.kr (H.W. Jang).

http://dx.doi.org/10.1016/j.snb.2015.02.103
0925-4005/

which is facile way to make various nanostructure depending on the shape of the sacrificial template [19,20]. Polystyrene or poly(methylmethacrylate) nanobeads are commonly used for sacrificial templates because they can be formed in close-packed arrays and easily removed by annealing at high temperatures, leading to highly ordered dome-like hollow structures [21]. These attractive advantages have already been identified them as the applications for high response metal oxide gas sensors [22]. Especially, the recent report by Dai et al. showed the utilization of monolayer polystyrene nanobeads templates on 4 inch Si wafer for highly sensitive gas sensors based on hollow metal oxide nanostructures [23].

Gas sensing properties of hollow metal oxide nanostructures can be enhanced by metal decoration on the surface because metal nanoparticles on the surface play as chemical and electronic sensitizers [24,25]. Generally, metal decoration on the surface of porous metal oxide nanostructures is performed using physical vapor deposition (PVD) of metal films and subsequent self-agglomeration into nanoparticles during the deposition or post-annealing, which leads to the relatively uniform coverage of metal nanoparticles on the surface and thermal stability for long-term operation compared to a drop coating method [26]. However, metal nanoparticles are formed only on the outer (top) surface of metal oxide nanostructures [24]. Consequently, both the outer and inner surface could not be utilized for metal decoration to further enhance the gas sensing properties. Therefore, a new method is necessary for enabling both the outer and inner surface of hollow metal oxide nanostructures to be functionalized by metal nanoparticles.

In this paper, in order to overcome the aforementioned limitation, we present a facile and effective strategy for the utilization of metal decoration on both the inner and outer surface of hollow metal oxide nanostructures using PVD for the first time. Highly ordered SnO_2 nanodome arrays with both-side Au decoration have been achieved using soft templates of polystyrene nanobeads. The deposition of an Au film is controlled to make the outer and/or inner surface of close-packed SnO_2 nanodome arrays decorated with Au nanoparticles and responses to various gases such as C_2H_5OH, H_2, CO, CH_4, C_7H_8, and CH_3COCH_3 have been measured at 300 °C. Our results show that the gas response of both-side Au-decorated SnO_2 nanodome arrays to ethanol is 18 times higher than that of bare SnO_2 nanodome arrays and the theoretical detection limit is below 1 ppb, which are mainly attributed to the formation of large-barrier double Schottky junctions between individual nanodomes.

2. Experimental

2.1. Fabrication

180-nm-thick Pt films were prepared on SiO_2/Si substrate using an electron beam evaporator at base pressure of 2×10^{-6} mTorr. Before Pt deposition, 20-nm-thick Ti was deposited for the good adhesion of Pt to the substrate. For gas sensor application, interdigitated electrode (IDE) patterns of 5 μm spacing were fabricated on the Pt/Ti films using photolithography and dry etching. The Pt-IDE-patterned SiO_2/Si substrate was treated by O_2 plasma using a microwave plasma etcher (Plasma Finish V15-G) at a working pressure of 400 mTorr (O_2) and an rf power of 150 W for 3 min to make the surface hydrophilic. An aqueous suspension of 700-μm-diameter polystyrene beads (2.6 wt%, Polysciences, Warrington, U.S.) was used to prepare a close-packed monolayer nanobead template on the Pt-IDE-patterned SiO_2/Si substrate via spin coating at a speed of 1000 rpm for 2 s. After the spin coating, the sample was dried for 1 h in a dry box at room temperature to evaporate the solution. Approximately a 2-nm-thick Au film was firstly deposited onto the monolayer nanobead template by an electron beam evaporator and then a 100-nm-thick SnO_2 film was deposited by a RF sputter using a polycrystalline SnO_2 target on the Au film deposited polystyrene monolayer template. The base pressure, working pressure, rf power, gas flow rate and growth rate were 2×10^{-6} mTorr, 10 mTorr, 100 W, 30 sccm (Ar) and 10 nm/min, respectively. A 2-nm-thick Au film was again deposited on the SnO_2-coated template. Finally, the sample was calcined in air at 550 °C for 1 h to burn out the polystyrene nanobeads and crystallize the SnO_2 film, which leads to the formation of SnO_2 nanodome arrays and simultaneously to the agglomeration of Au films to Au nanoparticles on both the inner and outer surface of SnO_2 nanodomes.

2.2. Characterization

The morphology of the fabricated SnO_2 nanodome arrays was characterized by an environmental scanning electron microscope (XL30 FEG ESEM, FEI) using an acceleration voltage of 15 kV and a working distance of 10 mm. Transmission electron microscopy (TEM) was performed using a JEM-2100F field emission transmission electron microscope (JEOL, Peabody, U.S.). For the TEM analysis, the specimen was prepared by mechanical polishing followed by ion milling with Ar ions (FIB, FEI-Helios).

2.3. Sensor measurements

Gas sensing properties of the Au-decorated SnO_2 nanodome arrays were measured in a quartz tube with external heating. The flow gas was changed from dry air to a calibrated target gas (balanced with dry air, Sinyang Gases). A constant flow rate of 500 sccm was used for the dry air and target gas. The response of the Au-decorated SnO_2 nanodome arrays was accurately determined by measuring the baseline resistance in dry air and the fully saturated resistance after exposure to the target gas. The resistances were measured at a DC bias voltage of 1 V using a source measurement unit (Keithley 236). The gas flow was controlled using mass flow controllers and all measurements were recorded on a computer using LabVIEW over the GPIB interface. Additional experimental details about sensor measurements may be found in our previous reports [24].

2.4. Calculation of theoretical detection limit

The detection limit could be derived from the sensor's signal processing performance. We took 10 resistance points at the baseline prior to an exposure to C_2H_5OH. And then a fifth-order polynomial fit was implemented within the data-point range, which gives both the curve-fitting equation and the statistical parameters of the polynomial fit.

$$Vx^2 = \sum (y_i - y)^2$$

where y_i is the measured data-point and y is the corresponding value calculated from the curve-fitting equation. The rms noise was calculated as

$$\mathrm{rms}_{\mathrm{noise}} = \sqrt{\frac{Vx^2}{N}}$$

where N is the number of data points used in the curve fitting. The theoretical detection limit (DL) could be calculated using the following equation.

$$\mathrm{DL(ppm)} = 3\left(\frac{\mathrm{rms}}{\mathrm{slope}}\right)$$

More details about calculation of theoretical detection limit may be found in previous report [27].

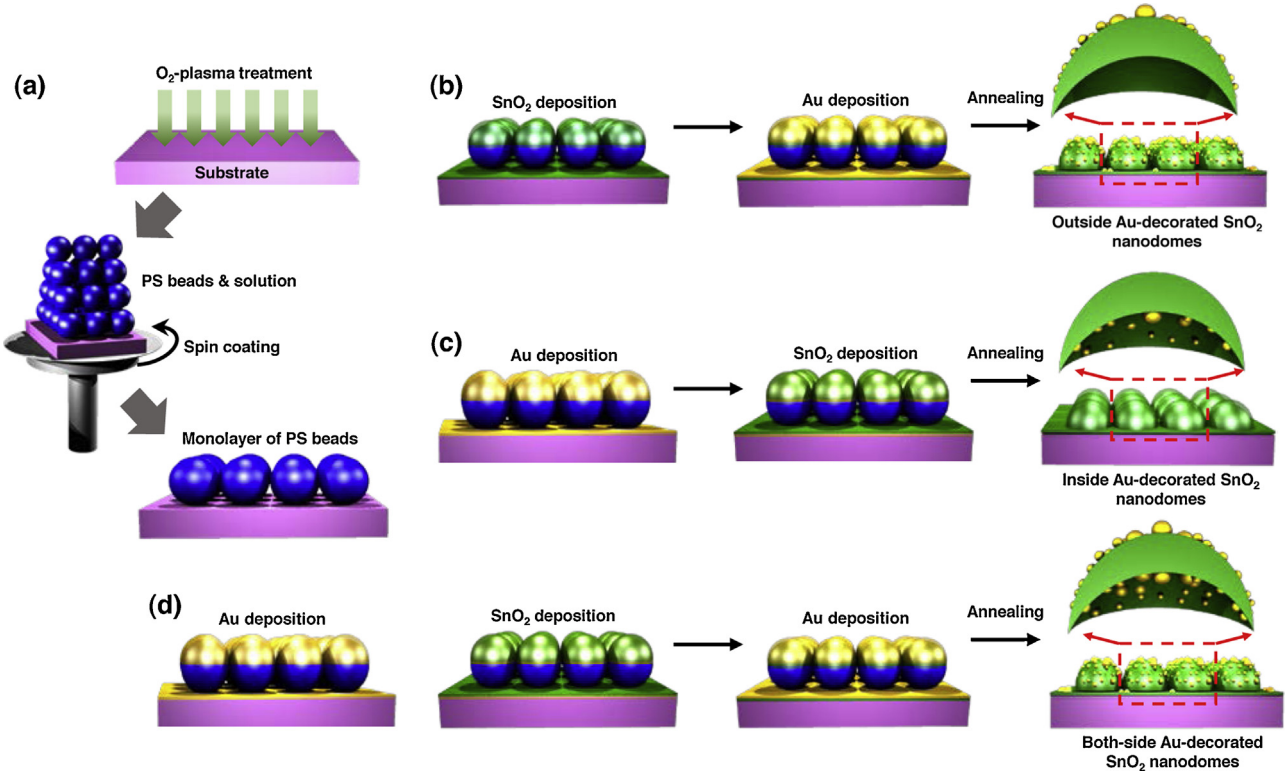

Fig. 1. Fabrication procedures for (a) monolayer of polystyrene beads, (b) outside, (c) inside, and (d) both-side Au-decorated SnO_2 nanodome arrays.

3. Results and discussion

The fabrication procedure of both-side Au-decorated close-packed SnO_2 nanodome arrays is illustrated in Fig. 1. Spin coating of an aqueous solution containing polystyrene nanobeads (700 nm in diameter) on a hydrophilic Pt-IDE-patterned SiO_2/Si substrate produced a close-packed monolayer of polystyrene nanobeads shown in Fig. 1(a). We could control the position of Au decoration for SnO_2 nanodome arrays by changing the deposition sequence of Au and SnO_2 films. For an outside Au-decorated SnO_2 nanodome arrays, a SnO_2 film was firstly deposited onto the polystyrene nanobeads and then an Au film was deposited on the SnO_2-coated polystyrene beads, as shown in Fig. 1(b). Reversely, we could obtain the inside Au-decorated SnO_2 nanodome arrays after an Au film was firstly deposited onto the polystyrene nanobeads and a SnO_2 film was sequentially deposited, as shown in Fig. 1(c). We note that the Au–SnO_2 adhesion is much stronger than the Au–polystyrene, which is the key to accomplish Au decoration on the inner surface of SnO_2 nanodome arrays. When the polystyrene nanobeads were burnt out during the calcination, the Au film was attached on the inner surface of SnO_2 nanodomes and simultaneously agglomerated to Au nanoparticles. For a both-side decorated SnO_2 nanodome arrays, we deposited Au films before and after the deposition of the SnO_2 film, as shown in Fig. 1(d). We used Pt IDEs with 5 μm spacing and 20 fingers as sensor electrodes. The area of the sensing film consisting of an Au-decorated SnO_2 nanodome arrays was approximately 1 mm × 1 mm, as shown in Fig. 2(a). The SEM image in Fig. 2(b) shows the plain view of both-side Au-decorated SnO_2 nanodome arrays on a Pt-IDE-patterned SiO_2/Si substrate. The active area between Pt finger electrodes was closely packed with both-side Au-decorated SnO_2 nanodomes without voids, aggregates and multilayers of nanodomes. Since the region between Pt IDEs is grooved, spin coating of the suspension resulted in the close packing of nanobeads between Pt IDEs. The high magnification SEM micrograph in Fig. 2(c) clearly shows surface morphology of a both-side Au-decorated SnO_2 nanodome arrays which is hexagonally close-packed with nanodomes and the distribution of Au nanoparticles is entirely uniform on the top surface.

In order to clarify Au decoration on the inner surface of SnO_2 nanodomes, Au-decorated SnO_2 nanodomes were scratched using a needle. The SEM image in Fig. 2(d) shows Au decoration on both the outer and inner surface of SnO_2 nanodomes. Au nanoparticles are uniformly distributed on the inside and outside of the SnO_2 nanodomes. Since the thicknesses of the Au films deposited inside and outside of the nanodomes are the same, the Au nanoparticle sizes on inside and outside of the nanodomes are also similar. Fig. 2(e) shows the SEM image of the substrate region where both-side Au-decorated SnO_2 nanodomes were detached. Au nanoparticles do not exist on the area originally occupied by SnO_2 nanodomes, indicating that Au nanoparticles were entirely attached to the inner surface of the SnO_2 nanodomes. In sharp contrast, Au nanoparticles exist in regions between individual nanodomes which are triangular. Cross-sectional TEM images of both-side Au-decorated SnO_2 nanodomes are shown in Fig. 2(f). The image clearly shows that the SnO_2 nanostructures are hollow and confirms both-side decoration with nanoparticles. Because the SnO_2 nanodome is hemispherical, Au nanoparticles gradually become smaller toward the bottom. Energy dispersive spectroscopy (EDS) element mapping confirmed both-side Au decoration, as shown in Fig. 2(g)–(i).

We have prepared bare, inside Au-decorated, and outside Au-decorated SnO_2 nanodome array samples to investigate the gas sensing properties of each samples. Generally, it is well known that the operating temperature has influence on gas sensing properties, since the oxygen ions, O_2^-, O^-, and O^{2-} are stable below 100 °C, between 100 and 300 °C and above 300 °C, respectively [28]. Correspondingly, various studies have reported that the response of n-type semiconducting gas sensor to reducing gases tends to increase as temperature increases, and decrease as temperature decreases [29]. In this study, operating temperature was fixed at 300 °C to vividly show the effect of the both-side Au decoration. All

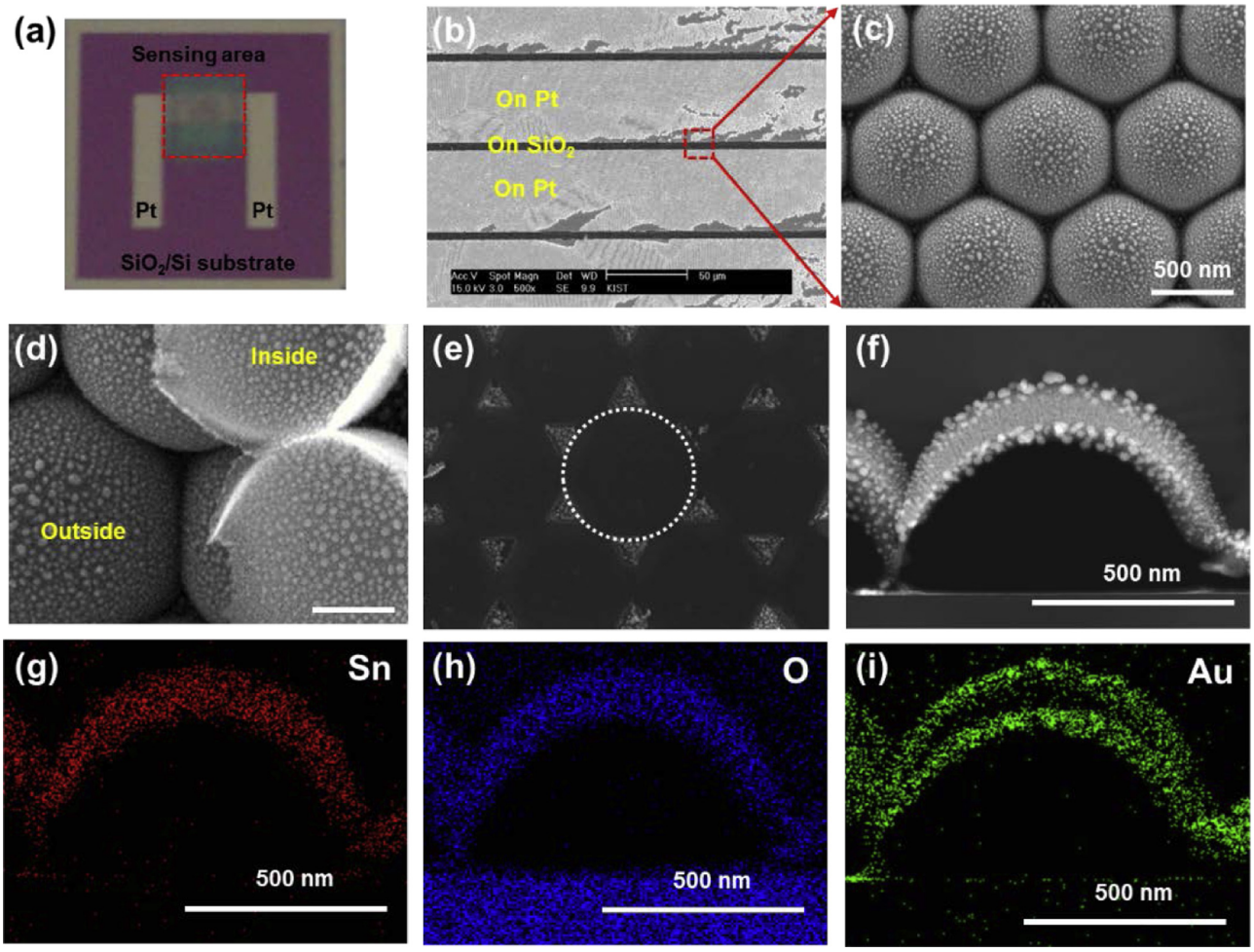

Fig. 2. (a) Photograph of the whole sensing device based on both-side Au-decorated SnO_2 nanodome arrays. (b) SEM micrograph of both-side Au-decorated SnO_2 nanodome arrays on Pt-IDE pattern SiO_2/Si substrate. (c) High magnification SEM image of the selected area in (b). (d) SEM micrograph of the inner and outer surface of both-side Au-decorated SnO_2 nanodomes. (e) SEM micrograph of a SiO_2/Si substrate after removing both-side Au-decorated SnO_2 nanodomes. The circle indicates the region where a SnO_2 nanodome existed before being removed. (f) Cross-sectional TEM image of both-side Au-decorated SnO_2 nanodomes. (g–i) EDS element maps of (g) Sn, (h) O and (i) Au for both-side Au-decorated SnO_2 nanodomes.

samples exhibit the different baseline resistances in air ambient, as shown in Fig. 3(a). The bare SnO_2 nanodome arrays show the lowest baseline resistance ($9.13 \times 10^3\ \Omega$) and the baseline resistance of the inside Au-decorated SnO_2 nanodome arrays ($5.8 \times 10^4\ \Omega$) is slightly higher than that of the outside Au-decorated SnO_2 nanodome arrays ($5.31 \times 10^4\ \Omega$). Both-side Au-decorated SnO_2 nanodomes exhibit the highest baseline resistance ($1.42 \times 10^5\ \Omega$). This indicates that large-barrier-height Schottky junctions were formed between Au nanoparticles and SnO_2, leading to increases in the base resistances due to the electronic sensitization effect [24], which was the strongest in the both-side Au-decoration sample. Upon exposure to 50 ppm C_2H_5OH, all samples exhibited instantaneous responses as their resistances decreased rapidly, revealing that SnO_2 is a typical n-type semiconductor. Fig. 3(b) shows responses of the samples (defined as $(R_{air} - R_{gas})/R_{gas}$, where R_{air} and R_{gas} denote resistance in the presence and the absence of a test gas, respectively) to 50 ppm C_2H_5OH at 300 °C. The responses of bare, inside Au-decorated, outside Au-decorated, and both-side Au-decorated SnO_2 nanodome arrays are 26.9, 176.9, 117.4, and 486.8, respectively. Excitingly, the both-side Au-decorated SnO_2 nanodome arrays exhibit the 18 times higher response than the bare SnO_2 nanodome. In our best knowledge, no work has demonstrated such a high response enhancement using metal decoration, which is much higher those of previously reported for high sensitivity sensors based on SnO_2 nanostructures with metal nanoparticles [30–35]. Another interesting result is that the response of inside Au-decorated sample is higher than that of the outside Au-decorated sample despite of the similar distribution of Au nanoparticles.

In order to identify the role of both-side Au-decoration on enhancing gas sensing properties of SnO_2 nanodome arrays to various gases, the responses of both-side Au-decorated SnO_2 nanodomes to various gases such as 50 ppm C_2H_5OH, H_2, CO, CH_4, C_7H_8, and CH_3COCH_3 have been measured. For comparison, the bare SnO_2 nanodome arrays were also tested. Response curves of bare and both-side Au-decorated SnO_2 nanodome arrays to the various gases are shown in Fig. 4(a) and (b). Responses of the both-side Au-decorated SnO_2 nanodome arrays to 50 ppm C_2H_5OH, H_2, CO, CH_4, C_7H_8, and CH_3COCH_3 at 300 °C are 486.8, 13.45, 3.66, 1.55, 63.74, and 79.3, respectively, while responses of the bare SnO_2 nanodome arrays are 26.9, 1.46, 0.72, 0.25, 7.17, and 15.62, respectively. Fig. 4(c) shows the polar plot of response ratios (S_a/S_b, S_a and S_b represent the responses of the bare and both-side Au-decorated SnO_2 nanodome arrays, respectively) to the various gases. The response ratios vary with the target gases. The response ratios for 50 ppm C_2H_5OH, H_2, CO, CH_4, C_7H_8, and CH_3COCH_3 are 18.1, 9.21, 5.08, 6.2, 8.88, and 5.07, respectively. This result shows that the gas sensing properties of SnO_2 nanodome arrays were significantly enhanced by both-side Au decoration, as shown in Fig. 4(d) and (e). Evidently,

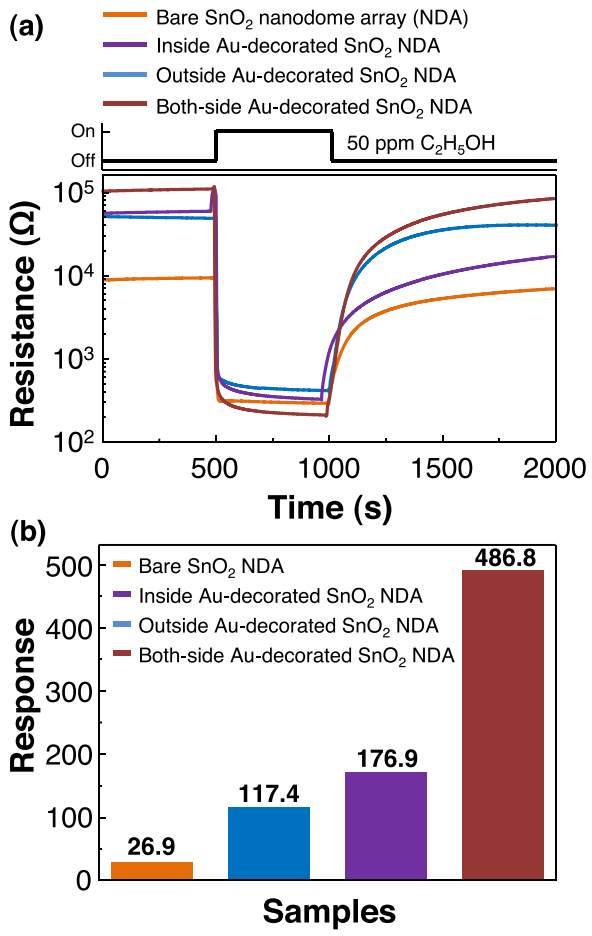

Fig. 3. (a) Response curves and (b) responses ($(R_{air} - R_{gas})/R_{gas}$) of bare, inside Au-decorated, outside Au-decorated and both-side Au-decorated SnO_2 nanodome arrays to 50 ppm C_2H_5OH at 300 °C.

we found that the both-side Au-decorated SnO_2 nanodome arrays exhibited an extremely high response to 50 ppm C_2H_5OH, indicating that the both-side Au-decorated SnO_2 nanodome arrays are beneficial for the selective detection of C_2H_5OH which is one of the most popular target gases for semiconductor gas sensors.

For practical applications, gas sensors are generally required to possess high stability upon long-term operation. The both-side Au-decorated SnO_2 nanodome arrays were repeatedly exposed to 50 ppm C_2H_5OH at 300 °C, as shown in Fig. 5(a). After the multiple exposures, the both-side Au-decorated SnO_2 nanodome arrays recover its original baseline resistance. Variations in the responses are less than 5%, suggesting that the both-side Au-decorated SnO_2 nanodome arrays could be subjected to long-term operation without degradation.

To check the linearity of the responses and evaluate the detection limit, the response of both-side Au-decorated SnO_2 nanodome arrays was measured over the range 1–5 ppm C_2H_5OH, as shown in Fig. 5(b). As the gas concentration increases, the response of the arrays increases. The responses of the nanodome arrays are 16.33, 25.01, 32.09, 38.1, and 44.85 to 1, 2, 3, 4, and 5 ppm C_2H_5OH, as shown in inset of Fig. 5(c). The responses of the both-side Au-decorated SnO_2 nanodome arrays are plotted as a function of the gas concentration on the logarithmic scale, as shown in Fig. 5(c). The linear relationship between the responses and C_2H_5OH concentrations indicates the reliable operation capability of the arrays over the concentration range. By applying linear least-squares fit to the data, the slope of the both-side Au-decorated SnO_2 nanodome arrays is determined to be 7.01 ppm^{-1}. Although the C_2H_5OH concentration of 1 ppm was the lowest examined experimentally in the present study, the theoretical detection limit (signal-to-noise ratio >3) is calculated to be extremely low as ~0.89 ppb for C_2H_5OH [27]. The sub-ppb level detection limit for C_2H_5OH demonstrates the potential of the both-side Au-decorated SnO_2 nanodome arrays for use in high performance C_2H_5OH sensors. Because C_2H_5OH (less than 0.1 ppm) is found in the breath of patients with lung cancer [6], we suggest that the both-side Au-decorated SnO_2 nanodome arrays using soft-template method are very promising for use in

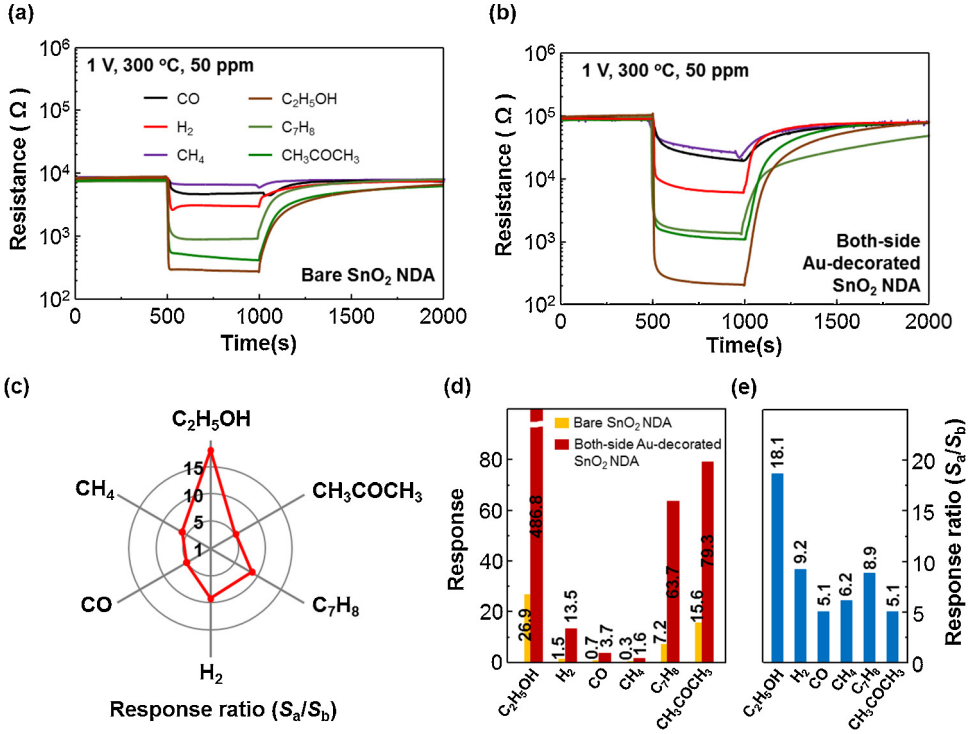

Fig. 4. Response curves of (a) bare SnO_2 nanodome arrays and (b) both-side Au-decorated SnO_2 nanodome arrays to 50 ppm C_2H_5OH, H_2, CO, CH_4, C_7H_8 and CH_3COCH_3. (c) Polar plot of response ratio (S_a/S_b) between bare SnO_2 nanodome arrays and both side Au-decorated SnO_2 nanodome arrays. (d) Responses and (e) response ratios.

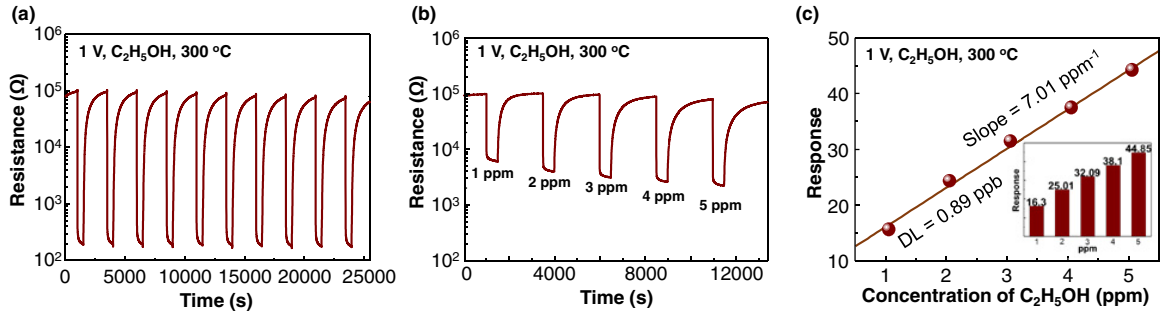

Fig. 5. The response curves to (a) pulses of 50 ppm C_2H_5OH and (b) toward 1–5 ppm C_2H_5OH. (c) Calibration of responses to 1–5 ppm C_2H_5OH.

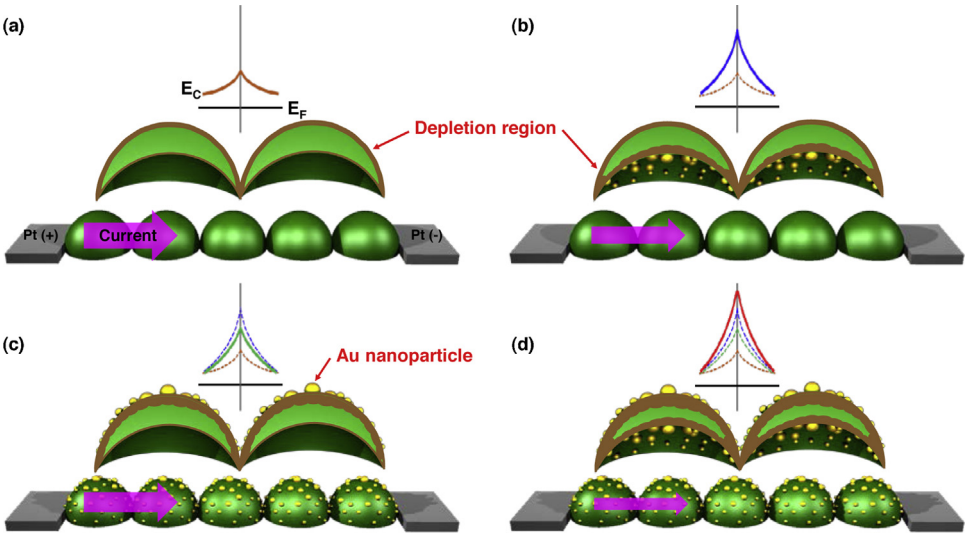

Fig. 6. Schematic drawings of the major current path between Pt electrodes for (a) bare SnO_2 nanodomes, (b) inside, (c) outside and (d) both-side Au-decorated SnO_2 nanodomes. The arrows indicate current flow and the size of each arrow denotes the magnitude of the current. The conduction band edges correspond to potential barriers in air.

high quality sensor materials for breath analysers to diagnose lung cancer.

It is apparent that Au decoration enhances gas sensing properties of SnO_2 nanodome arrays owing to two sensitizations such as electronic and chemical sensitizations [26,36,37], which have been already reported in our previous studies [24,25]. The underlying mechanism for the response enhancement by both-side Au decoration is described with schematics in Fig. 6. The modulation of barrier potentials in links between individual SnO_2 nanodomes upon exposure to a target gas determines the response of the sample [21]. As illustrated in Fig. 6(a)–(d), the both-side Au-decorated sample shows the highest barrier potential. The difference in baseline resistances for the samples in Fig. 3(a) is attributed to the formation of Schottky junctions between Au nanoparticles and SnO_2. Upon exposure to air ambient, the adsorbed oxygen ions form electron-depleted region on the surface of SnO_2. The effective depth of the enhanced electron-depleted region in the bare SnO_2 nanodome is shallower than in the inside, outside and both-side Au-decorated SnO_2 nanodome arrays since Au–SnO_2 Schottky junctions make the depletion layer thicker [24]. When the SnO_2 nanodome arrays were exposed to air, the outer surface is more electron-depleted due to oxygen adsorption. Gas diffusion to the inner surface of the nanodomes hardly happens, which has already been shown in our previous study [21]. However, the inside of SnO_2 nanodomes could be more electron-depleted by Au decoration for the inside Au-decorated SnO_2 nanodome arrays. Even though the outside Au-decorated sample has the thicker depletion layer on the outer surface, the total thickness of the depletion layers on both the outer and inner surface would be larger in the inside Au-decorated sample, resulting in the higher response. In this respect, the total thickness of the depletion layers on both the outer and inner surface should be the largest in the both-side decorated sample, leading to the ultrahigh response to various gases undoubtedly. In other words, the both-side decoration leads to the maximized electronic sensitization effect in the given geometric configuration.

4. Conclusion

Highly ordered and close-packed both-side Au-decorated SnO_2 nanodome arrays were fabricated using soft-template method and self-agglomeration. The responses of the both-side Au-decorated SnO_2 nanodome arrays to various gases such as 50 ppm C_2H_5OH, H_2, CO, CH_4, C_7H_8, and CH_3COCH_3 were much higher than those of bare SnO_2 nanodome arrays. Especially, the gas response of the both-side Au-decorated SnO_2 nanodome arrays to 50 ppm C_2H_5OH was 18 times higher than that of the bare SnO_2 nanodome arrays. The theoretical detection limit to C_2H_5OH was below 1 ppb, which indicates the promising potential application of the both-side Au-decorated SnO_2 nanodome arrays to breath analysers to diagnose lung cancer from exhaled breath. These results were attributed to the extreme utilization of the electronic sensitization by Au decoration on both the inner and outer surface of SnO_2 nanodomes. We strongly believe that our method is very suitable to make high performance gas sensor arrays. Just by changing the outside decoration such as Au, Pt, Pd, and Ag, different sensing elements for selective gas sensing can be produced. We suggest that the

both-side decoration can be applied to not only various metal oxide nanostructures but also to 2-dimensional nanomaterials such as graphene and transition metal dichalcogenides. The facileness, large-scale productivity and compatibility with semiconductor production processes hold promise for future applications including photocatalysts and solar cells where Au nanoparticles play a role due to catalytic and plasmonic effects.

Acknowledgements

This work was financially supported by the Center for Integrated Smart Sensors funded by the Ministry of Science, ICT & Future Planning as the Global Frontier Project, the Fusion Research Program for Green Technologies and the Outstanding Young Researcher Program (2013R1A1A1005928) through the National Research Foundation of Korea, the Aspiring Researcher Program through Seoul National University in 2013 and a research program of the Korea Institute of Science and Technology.

References

[1] N. Yamazoe, Toward innovations of gas sensor technology, Sens. Actuators B 187 (2013) 162–167.
[2] I.D. Kim, H.L. Tuller, Advances and new direction in gas-sensing device, Acta Mater. 61 (2013) 974–1000.
[3] S. Hwang, H. Kwon, S. Chhajed, J.W. Byon, J.M. Baik, J. Im, S.H. Oh, H.W. Jang, S.J. Yoon, J.K. Kim, A near single crystalline TiO_2 nanohelix array: enhanced gas sensing performance and its application as a monolithically integrated electronic nose, Analyst 138 (2012) 443–450.
[4] H.G. Moon, Y.S. Shim, D.H. Kim, H.Y. Jeong, M. Jeong, J.Y. Jung, S.M. Han, J.K. Kim, J.S. Kim, H.H. Park, J.H. Lee, H.L. Tuller, S.J. Yoon, H.W. Jang, Self-activated ultrahigh chemosensitivity of oxide thin film nanostructures for transparent sensors, Sci. Rep. 2 (2012) 588.
[5] N. Chérot-Kornobis, S. Hulo, J.L. Edmé, V. de Broucker, R. Matran, A. Sobaszek, Analysis of nitrogen oxides (NO_x) in the exhaled breath condensate (EBC) of subjects with asthma as a complement to exhaled nitric oxide (FeNO) measurements: a cross-sectional study, BMC Res. Notes 4 (2011) 202.
[6] R.F. Machado, D. Laskowski, O. Deffenderfer, T. Burch, S. Zheng, P.J. Mazzone, T. Mekhail, C. Jennings, J.K. Stoller, J. Pyle, J. Duncan, R.A. Dweik, S.C. Erzurum, Detection of lung cancer by sensor array analyses of exhaled breath, Am. J. Respir. Crit. Care Med. 171 (2005) 1286–1291.
[7] A.D. Smith, J.O. Cowan, S. Filsell, C. McLachlan, G. Monti-Sheehan, P. Jackson, D.R. Taylor, Comparisons between exhaled nitric oxide measurements and conventional tests, Am. J. Respir. Crit. Care Med. 169 (2004) 473.
[8] D.H. Kim, Y.S. Shim, H.G. Moon, H.J. Chang, D. Su, S.Y. Kim, J.S. Kim, B.K. Ju, S.J. Yoon, H.W. Jang, Highly ordered TiO_2 nanotubes on patterned substrates: synthesis-in-place for ultrasensitive chemiresistors, J. Phys. Chem. C 117 (2013) 17824–17831.
[9] K.I. Choi, H.J. Kim, Y.C. Kang, J.H. Lee, Ultraselective and ultrasensitive detection of H_2S in highly humid atmosphere using CuO-loaded SnO_2 hollow spheres for real-time diagnosis of halitosis, Sens. Actuators B 194 (2014) 371–376.
[10] N.H. Kim, S.J. Choi, D.J. Yang, J. Bae, J. Park, I.D. Kim, Highly sensitive and selective hydrogen sulfide and toluene sensors using Pd functionalized WO_3 nanofibers for potential diagnosis of halitosis and lung cancer, Sens. Actuators B 193 (2014) 574–581.
[11] U. Tisch, H. Haick, Chemical sensors for breath gas analysis: the latest developments at the breath analysis summit 2013, J. Breath Res. 8 (2014) 027103.
[12] J.R. Askim, M. Mahmoudi, K.S. Suslick, Optical sensor arrays for chemical sensing: the optoelectronic nose, Chem. Soc. Rev. 42 (2013) 8649–8682.
[13] M. Csete, W.D. Hunt, Potential of surface acoustic wave biosensors for early sepsis diagnosis, J. Clin. Monit. Comput. 27 (2013) 427–431.
[14] N. Barsan, D. Koziej, U. Weimar, Metal oxide-based gas sensor research: how to? Sens. Actuators B 30 (2007) 18–35.
[15] K.J. Choi, H.W. Jang, One-dimensional oxide nanostructures as gas-sensing materials: review and issues, Sensors 10 (2010) 4083–4099.
[16] J.H. Lee, Gas sensors using hierarchical and hollow oxide nanostructures: overview, Sens. Actuators B 140 (2009) 319–336.
[17] S.J. Pearton, F. Ren, Y.L. Wang, B.H. Chu, K.H. Chen, C.Y. Chang, W. Lim, J. Lin, D.P. Norton, Recent advances in wide bandgap semiconductor biological and gas sensors, Prog. Mater. Sci. 55 (2010) 1–59.
[18] Y. Qin, G. Fan, K. Liu, M. Hu, Vanadium pentoxide hierarchical structure networks for high performance ethanol gas sensor with dual working temperature characteristic, Sens. Actuators B 190 (2014) 141–148.
[19] I.D. Kim, A. Rothschild, T. Hyodo, H.L. Tuller, Microsphere templating as means of enhancing surface activity and gas sensitivity of $CaCu_3Ti_4O_{12}$ thin films, Nano Lett. 6 (2006) 193–198.
[20] Y.E. Chang, D.Y. Youn, G. Ankonina, D.J. Yang, H.G. Kim, A. Rothschild, I.D. Kim, Fabrication and gas sensing properties of hollow SnO_2 hemispheres, Chem. Commun. 27 (2009) 4019–4021.
[21] H.G. Moon, Y.S. Shim, D. Su, H.H. Park, S.J. Yoon, H.W. Jang, Embossed TiO_2 thin films with tailored links between hollow hemispheres: synthesis and gas-sensing properties, J. Phys. Chem. C 115 (2011) 9993–9999.
[22] H.G. Moon, Y.S. Shim, H.W. Jang, J.S. Kim, K.J. Choi, C.Y. Kang, J.W. Choi, H.H. Park, S.J. Yoon, Highly sensitive CO sensors based on cross-linked TiO_2 hollow hemispheres, Sens. Actuators B 149 (2010) 116–121.
[23] Z. Dai, L. Xu, G. Duan, T. Li, H. Zhang, Y. Li, Y. Wang, Y. Wang, W. Cai, Fast-response, sensitive and low-power chemosensors by fusing nanostructured porous thin film and IDEs-microheater chip, Sci. Rep. 3 (2014) 1669.
[24] Y.S. Shim, H.G. Moon, D.H. Kim, L. Zhang, S.J. Yoon, Y.S. Yoon, C.Y. Kang, H.W. Jang, Au-decorated WO_3 cross-linked nanodomes for ultrahigh sensitive and selective sensing of NO_2 and C_2H_5OH, RSC Adv. 3 (2013) 10452.
[25] Y.S. Shim, L. Zhang, D.H. Kim, Y.H. Kim, Y.R. Choi, S.H. Nahm, C.Y. Kang, W. Lee, H.W. Jang, Highly sensitive and selective H_2 and NO_2 gas sensor based on surface-decorated WO_3 nanoigloos, Sens. Actuators B 198 (2014) 294–301.
[26] A. Kolmakov, D.O. Klenov, Y. Lilach, S. Stemmer, M. Moskovits, Enhanced gas sensing by individual SnO_2 nanowires and nanobelts functionalized with Pd catalyst particles, Nano Lett. 5 (2005) 667–673.
[27] J. Li, Y. Lu, Q. Ye, M. Cinke, J. Han, M. Meyyappan, Carbon nanotube sensor for gas and organic vapor detection, Nano Lett. 7 (2003) 929–933.
[28] K. Wetchakun, T. Samerjai, N. Tamaekong, C. Liewhiran, C. Siriwong, V. Kruefu, A. Wisitsoraat, A. Tuantranont, S. Phanichphant, Semiconducting metal oxides as sensors for environmentally hazardous gases, Sens. Actuators B 160 (2011) 580–591.
[29] B.L. Zhu, C.S. Xie, W.Y. Wang, K.J. Huang, J.H. Hu, Improvement in gas sensitivity of ZnO thick film to volatile organic compounds (VOCs) by adding TiO_2, Mater. Lett. 58 (2004) 624–629.
[30] C. Jin, H. Kim, S. Park, H.W. Kim, S. Lee, C. Lee, Enhanced ethanol gas sensing properties of SnO_2 nanobelts functionalized with Au, Ceram. Int. 38 (2012) 6585–6590.
[31] I.S. Hwang, J.K. Choi, H.S. Woo, S.J. Kim, S.Y. Jung, T.Y. Seong, I.D. Kim, J.H. Lee, Facile control of C_2H_5OH sensing characteristics by decorating discrete Ag nanoclusters on SnO_2 nanowire networks, ACS Appl. Mater. Interfaces 3 (2011) 3140–3145.
[32] J. Zhang, X. Liu, S. Wu, M. Xu, X. Guo, S. Wang, Au nanoparticle-decorated porous SnO_2 hollow spheres: a new model for a chemical sensor, J. Mater. Chem. 20 (2010) 6453–6459.
[33] A. Tricoli, M. Graf, S.E. Pratsinis, Optimal doping for enhanced SnO_2 sensitivity and thermal stability, Adv. Funct. Mater. 18 (2008) 1969–1976.
[34] X. Liu, J. Zhang, X. Guo, S. Wu, S. Wang, Enhanced sensor response of Ni-doped SnO_2 hollow spheres, Sens. Actuators B 152 (2011) 162–167.
[35] S.J. Choi, M.P. Kim, S.J. Lee, B.J. Kim, I.D. Kim, Facile Au catalyst loading on the inner shell of hollow SnO_2 spheres using Au-decorated block copolymer sphere templates and their selective H_2S sensing characteristics, Nanoscale 6 (2014) 11898–11903.
[36] J.M. Baik, M. Zielke, M.H. Kim, K.L. Turner, A.M. Wodtke, M. Moskovits, Tin-oxide-nanowire-based electronic nose using heterogeneous catalysis as a functionalization strategy, ACS Nano 4 (2010) 3117–3122.
[37] X.H. Chen, M. Moskovits, Observing catalysis through the agency of the participating electrons: surface-chemistry-induced current changes in a tin oxide nanowire decorated with silver, Nano Lett. 3 (2007) 807–812.

Biographies

Young-Seok Shim is studying for his Ph.D. course in the Department of Materials Science and Engineering of Yonsei University, and is an assistant researcher in Research Institute of Advanced Materials. His research interests include fabrication of metal oxide thin films, metal catalyst and their applications to functional devices.

Do Hong Kim is studying for his Ph.D. course in the Department of Materials Science and Engineering of Korea University. His research interests include the synthesis of nanostructured metal oxide thin films and their electrical and optical characteristics.

Hu Young Jeong received his PhD. from the Department of Materials Science and Engineering of KAIST in 2010. Now he is an assistant professor at UNIST Central Research Facilities of UNIST. His research interests include the material characterization using advanced transmission electron microscope such as a spherical-aberration (Cs) corrected TEM.

Yeon Hoo Kim is studying for his Ph.D. course in the Department of Materials Science and Engineering of Seoul National University. Her research interests include the fabrication of metal oxide nanostructures and their applications to functional devices.

Seung Hoon Nahm received his Ph.D. degree in Mechanical Engineering from Kyungbook National University in 1996. He is currently a principal researcher at Korea Research Institute of Standards and Science. His research interests include development of multi-mode sensing technology for harmful substances based on nano-web.

Chong-Yun Kang received his Ph.D. from the Department of Electrical Engineering of Yonsei University in 2000. Now he is a principal research scientist in KIST and a professor of KU-KIST Graduate School of Converging Science and Technology in Korea University. His research interests include embedded passive components in SOP, piezoelectric actuators, and gas sensors.

Jin-Sang Kim received his Ph.D. from the Department of Materials Science and Engineering of Seoul National University in 1997. Now he is a principal research scientist in KIST. His research interests include synthesis of electronic materials and their applications into sensors and optoelectronic devices.

Wooyoung Lee is a professor of Department of Materials Science and Engineering, the chairman of Yonsei Institute of Convergence Technology and the Head of Institute of Nanoscience and Nanotechnology at Yonsei University in Korea. He received a BS degree in metallurgical engineering in 1986, a MS degree in metallurgical engineering from the Yonsei University in 1988. He received a Ph.D. degree in physics from University of Cambridge, England in 2000. He is an advisor in National Assembly Research Service. In recent years, his research interests have centered on thermoelectric materials and devices, hard magnetic materials, hydrogen sensors and hydrogen storage materials. He has authored and co-authored over 150 publications, and has edited several of special books on nanostructured materials and devices.

Ho Won Jang received his Ph.D. from the Department of Materials Science and Engineering of POSTECH in 2004. He joined the Department of Materials Science and Engineering of Seoul National University in 2012 as an assistant professor. His research interests are the synthesis of nanostructured oxide thin films and their applications to various devices including sensors, solar water splitting cells, light-emitting diodes, photovoltaics, and memristors.